Determination of the size distribution of metallic nanoparticles by optical extinction spectroscopy

Ovidio Peña,[1,*] Luis Rodríguez-Fernández,[2] Vladimir Rodríguez-Iglesias,[2] Guinther Kellermann,[3] Alejandro Crespo-Sosa,[2] Juan Carlos Cheang-Wong,[2] Héctor Gabriel Silva-Pereyra,[2] Jesús Arenas-Alatorre,[2] and Alicia Oliver[2]

[1]Instituto de Investigaciones en Materiales, Universidad Nacional Autónoma de México, Circuito Exterior S/N, Ciudad Universitaria, Coyoacan, C.P. 04510, México, D.F., México

[2]Instituto de Física, Universidad Nacional Autónoma de México, Apartado Postal 20-364, México, D.F., 01000, México

[3]Laboratório Nacional de Luz Síncrotron (LNLS), Campinas, SP, Brazil

*Corresponding author: ovidio@bytesfall.com

Received 14 November 2008; revised 17 December 2008; accepted 19 December 2008; posted 19 December 2008 (Doc. ID 104084); published 15 January 2009

A method is proposed to estimate the size distribution of nearly spherical metallic nanoparticles (NPs) from optical extinction spectroscopy (OES) measurements based on Mie's theory and an optimization algorithm. The described method is compared against two of the most widely used techniques for the task: transmission electron microscopy (TEM) and small-angle x-ray scattering (SAXS). The size distribution of Au and Cu NPs, obtained by ion implantation in silica and a subsequent thermal annealing in air, was determined by TEM, grazing-incidence SAXS (GISAXS) geometry, and our method, and the average radius obtained by all the three techniques was almost the same for the two studied metals. Concerning the radius dispersion (RD), OES and GISAXS give very similar results, while TEM considerably underestimates the RD of the distribution. © 2009 Optical Society of America

OCIS codes: 160.3900, 160.4236, 290.2200, 290.4020, 300.1030.

1. Introduction

Metallic nanoparticles (NPs) embedded in glass matrices present linear and nonlinear optical properties that are very promising for technological applications in different fields such as catalysis [1], optoelectronics [2–5], and biomedical diagnosis using dark field light microscopy [6,7]. For optical applications, silica is one of the most commonly used host metallic NPs materials due to its exceptional high transparency in a wide spectral region (visible–UV) and low conductivity. There are several experimental methods of synthesis of metal NPs in a glass matrix, but ion implantation followed by an additional thermal annealing has proven to be a very useful method to obtain large volume fractions of NPs in a well-defined depth below the surface, which can be chosen by means of the ion energy [8]. Additional advantages of ion implantation are controllability of depth profile and concentration, high purity, and the possibility to overcome low solubility restrictions. Particularly, deep ion implantation using energies of the order of MeV produces an ion depth distribution located some micrometers underneath the surface and wide enough to be convenient to produce optical waveguides.

Nevertheless, technological applications require reliable methods to produce the NPs under controlled conditions, because their optical properties depend on several factors such as size, shape, spatial distribution, and interaction with the host matrix, with the average size and size dispersion being some of the most influencing (and hardest to study/control)

0003-6935/09/030566-07$15.00/0

of these factors. Therefore it is of paramount importance to be able to determine the size distribution of NPs in an easy, reliable way.

Several methods have been used to achieve this goal, with transmission electron microscopy (TEM), small-angle x-ray scattering (SAXS), grazing-incidence SAXS (GISAXS), and optical extinction spectroscopy (OES) being some of the most commonly employed. In general, OES is preferred, because it is nondestructive and the results can be obtained rapidly. Additionally, TEM has the limitations that sample preparation can be quite difficult due to the mechanical properties of the silica matrix, and in some cases, the method used for sample preparation can induce changes in the characteristics of the NPs. Besides, only a small region of the sample is studied, leading to results that could not be representative of the whole sample. On the other hand, SAXS is restricted by the sample thickness and GISAXS by the depth of the NPs below the surface sample. The problem with OES is that obtaining the size distribution from the experimental results is a task far from trivial. Usually the electrostatic approximation [9] is used to overcome this problem, because an explicit equation for the extinction coefficient is obtained, which can then be easily fitted to the experimental results. But this method has the disadvantage that the electrostatic approximation is only valid for very small NPs (<10 nm), and therefore the results are no reliable if larger NPs are present in the sample. Some other approximations [10–12] exhibit similar restrictions with respect to the range of sizes in which they are useful for sizing the particles.

In this work, we propose a method to obtain the average size and size dispersion of metallic NPs using the Mie theory coupled with the bounded limited memory Broyden–Fletcher–Goldfarb–Shanno (L-BFGS-B) [13–15] multivariate optimization algorithm. Compared with the methods based in the electrostatic approximation, our procedure requires more complex calculations, but this can be handled easily by any modern computer, and it has the advantage that it is valid for NPs of any size. This algorithm is applied to the size distribution characterization of Cu and Au NPs embedded in silica synthesized by ion implantation. The results are compared to measurements done by TEM and GISAXS.

2. Fitting Algorithm

A. Optical Density

It is necessary, before comparing the experimental results and the simulations, to compute the optical density (OD), which is the quantity obtained from the spectrophotometer. The transmission (I/I_{inc}) and the extinction coefficient α for a sample of length l are related by [16,17]

$$\begin{aligned} \alpha l &= \ln\left(\frac{I_{\mathrm{inc}}}{I}\right) = \log^{-1}(e)\cdot\log\left(\frac{I_{\mathrm{inc}}}{I}\right) \\ &= \log^{-1}(e)\cdot \mathrm{OD}, \end{aligned} \tag{1}$$

where I_{inc} and I are incident and transmitted intensities, respectively. The extinction coefficient, in turn, is derived from the extinction cross section (σ_{ext}) : $\alpha = N\sigma_{\mathrm{ext}}$, where N is the number of NPs in a volume unit; and so OD can be obtained as

$$\mathrm{OD} = \log(e) N l \sigma_{\mathrm{ext}} = \log(e)\frac{f}{Vd}\sigma_{\mathrm{ext}}, \tag{2}$$

where V is the volume of the NP, d is the atomic density $(\mathrm{at/cm^3})$, and f is the implanted fluence of the sample $(\mathrm{at/cm^3})$. Finally the extinction cross section is the quantity obtained from most of Mie's implementations. Specifically for this work, we used an implementation [18] based on Yang's algorithm [19] (this algorithm is for a multilayered sphere but reduces to normal Mie theory if only one layer is used, as in our case).

Now we have to obtain an expression for the OD of an ensemble of NPs averaged over a distribution of sphere radii $n(r)$, and the ensemble-averaged OD based on Eq. (2) is relatively straightforward [20]:

$$\langle \mathrm{OD}\rangle = \log(e)\frac{f}{\langle V\rangle d}\langle\sigma_{\mathrm{ext}}\rangle, \tag{3a}$$

$$\langle\sigma_{\mathrm{ext}}\rangle = \int_{r_{\min}}^{r_{\max}} n(r)\sigma_{\mathrm{ext}}(r)\mathrm{d}r = \sum_{i=1}^{N_r} u_i n(r_i)\sigma_{\mathrm{ext}}(r_i), \tag{3b}$$

$$\langle V\rangle = \frac{4}{3}\pi\int_{r_{\min}}^{r_{\max}} n(r)r^3\mathrm{d}r = \frac{4}{3}\pi\sum_{i=1}^{N_r} u_i n(r_i) r_i^3, \tag{3c}$$

where $\langle\sigma_{\mathrm{ext}}\rangle$ and $\langle V\rangle$ are the ensemble-averaged extinction cross section and volume, respectively, while r_i and u_i are the division points and weights of a quadrature formula on the interval $[r_{\min}, r_{\max}]$. For this work, a normal distribution of radii was used:

$$n(r) = C\times\exp\left(-\frac{(r-r_n)^2}{2\sigma_n^2}\right), \tag{4}$$

where r_n and σ_n are the mean and standard deviation of the distribution, respectively, and the constant C was chosen such that the size distribution satisfies the standard normalization condition $(\Sigma n(r_i) = 1)$.

B. L-BFGS-B Algorithm

We will only give a brief outline of the L-BFGS-B algorithm, but for a more detailed description, see [13–15]. This method is a limited-memory quasi-Newton algorithm for solving large nonlinear optimization problems with simple bounds on the variables. The problem can be written as

$$\min[f(x)]\, l \le x \le u, \tag{5}$$

where $f : R^n \to R$ is a nonlinear function whose gradient g is available, the vectors l and u represent lower and upper bounds on the variables, and the number of variables n is assumed to be large (but the method can be used for small dimension problems too). The algorithm does not require second derivatives or knowledge of the structure of the objective function and can therefore be applied when the Hessian matrix is not practical to compute. Instead of that, the Hessian is generated on the basis of the N consequent gradient calculations, and then the quasi-Newton step is performed. On each approximation step, the matrix remains positive definite, and the gradient projection method is used to determine a set of active constraints.

C. Optimization

For the optimization process, we used the chi-square distribution as the objective function:

$$\chi^2(r_n, \sigma_n, n_{\text{matrix}}, f) = \frac{1}{N}\sum_{i=1}^{N} \frac{(\langle \text{OD}\rangle^i(\lambda_i, r_n, \sigma_n, n_{\text{matrix}}, f) - \text{OD}^i_{\text{exp}})^2}{\text{OD}^i_{\text{exp}}}, \quad (6)$$

where N is the number of points used for the fit, n_{matrix} is the refractive index of the matrix, and OD^i_{exp} are the values of the experimental OD. Then, starting with the given initial values of the variables to optimize ($X_k = r_n, \sigma_n, n_{\text{matrix}}$) and the experimental OD, several optimization steps are performed iteratively; in each of them, the value of χ^2 and its gradient G are calculated, and subsequently the L-BFGS-B algorithm is applied to obtain a new "optimized" value for all the variables X_k. Lower and/or upper limits are set for all the variables in order to ensure that their optimized values have physical meaning (e.g., positive radii). The optimization process is finished when one of the following criteria is met:

$$\|G_k\| \le \varepsilon_G, \quad (7a)$$

$$|(\chi^2)^{(i+1)} - (\chi^2)^{(i)}| \le \varepsilon_F \cdot \max\{(\chi^2)^{(i)}, (\chi^2)^{(i+1)}, 1\}, \quad (7b)$$

$$|X_k^{(i+1)} - X_k^{(i)}| \le \varepsilon_X, \quad (7c)$$

where ε_G, ε_F, and ε_X are positive numbers that define a precision of search, $\|\cdot\|$ means Euclidian norm, G_k, gradient projection onto a variable X_k, and the super index represents the iteration number. Additionally, the optimization can be finished after a certain number of iterations. For the fittings presented in this work, no limit was set for the number of iterations, and the precision of search was taken as $\varepsilon_G = \varepsilon_F = \varepsilon_X = 1 \times 10^{-10}$.

3. Experimental

The sample host matrix consisted in 20 mm × 20 mm × 1 mm squares of high-purity silica glass type ED-C grade made by Nippon Silica Glass, with OH content lower than 1 ppm and a total impurity content of less than 20 ppm. These plates were implanted with either 2 MeV Cu or 2 MeV Au ions at room temperature, keeping the beam current density below 100 nA/cm^2 during all the process in order to avoid thermal effects in the ion depth profile distribution. The irradiations were done at normal incidence for gold and at a tilt angle of 60° for copper, using the Pelletron tandem accelerator at the Instituto de Física, UNAM. Fluences of 6.6×10^{16} and 4.4×10^{16} ions/cm^2 were used for Au and Cu, respectively. After implantation, the samples were cut into identical small pieces, keeping some of them as as-implanted references, and the others were annealed at a temperature of 900 °C for 1 h in air.

Ion depth profile distributions were determined by Rutherford backscattering spectrometry (RBS) with ^{4}He ions in the 2–3 MeV energy range. Optical absorption measurements were performed at room temperature using a Cary 500 double-beam spectrophotometer in the 300–800 nm wavelength range before and after the thermal annealing. TEM studies were performed in a JEOL-2010 FEG instrument with a point-to-point resolution of 1.9 Å. Based on a multilayer sample preparation, the TEM samples were prepared using a tripod polisher to generate a cross-section sample with a final thickness <100 nm,

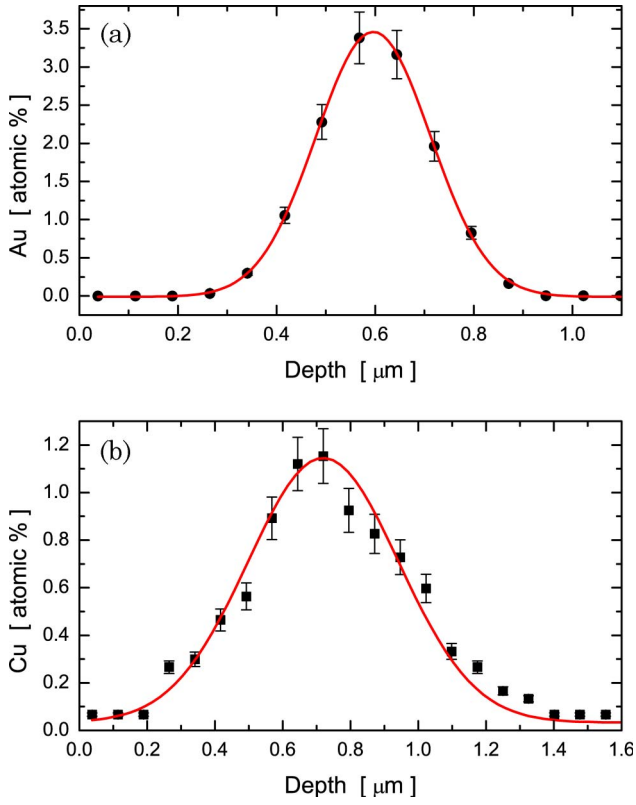

Fig. 1. (Color online) Depth profile distributions obtained for (a) Au and (b) Cu from fitting the RBS spectra. The continuous curves (red) correspond to best fitting to experimental data assuming Gaussian functions.

enough to be transparent to the electron beam. From the TEM images, we calculated the particle size distribution of the samples.

The samples were also analyzed by GISAXS using a monochromatic 8 keV x-ray beam at the XRD2 beam line of the Brazilian National Synchrotron Light Laboratory in Campinas, Brazil. The dispersion patterns were determined with the IsGISAXS v2.6 software [21]. For the calculation of the theoretical OES spectra, bulk dielectric function values of Cu and Au reported by Johnson and Christy [22] were used after applying a correction to incorporate surface dispersion effects [23]. A background (assumed to be the OD of unimplanted silica) was added to the simulated spectra. The size distributions obtained from TEM, GISAXS, and the fitting procedure described earlier were compared to determine the accuracy of our method.

4. Results and Discussion

From the RBS analysis, it was found that the ion depth distribution into the silica was close to a Gaussian in both the Au and the Cu implanted samples (Fig. 1). For the first ones, the maximum concentration is located at 0.57 μm from the surface sample, with a full-width at half-maximum (FWHM) of 0.28 μm, while in the second group of samples, the maximum concentration is at 0.72 μm, with a FWHM of 0.52 μm. The bimodal distribution that has been previously reported for Cu [24] was not observed in this case. No significant changes were observed in the RBS spectra of the samples before and after the thermal annealing, showing that the diffusion effects are negligible during this process.

From low resolution micrographs, like the ones shown in Figs. 2(a) and 2(b), the size distribution in the samples were determined (around 150

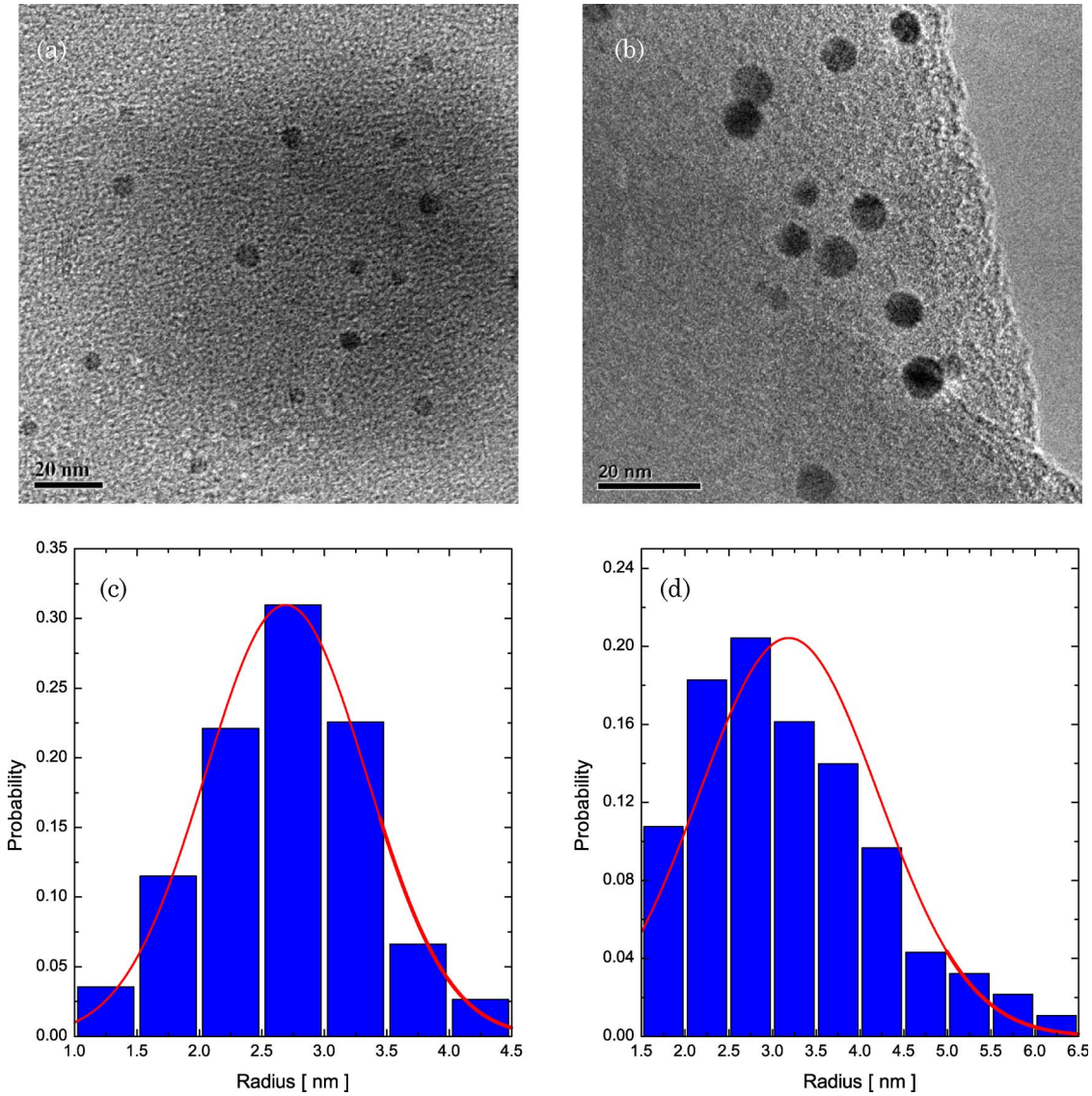

Fig. 2. (Color online) Low magnification TEM micrographs obtained for (a) Au and (b) Cu NPs and (c) and (d) their corresponding probability histograms, respectively, obtained from the analysis of TEM images.

particles were analyzed in each case). The radii distribution histograms [Figs. 2(c) and 2(d)] show an acceptable agreement with a normal distribution with an average radius (AR) of 2.8 nm and radius dispersion (RD) of 1.6 nm for Au and an AR of 3.2 nm and RD of 2.5 nm for Cu. The samples were also analyzed using GISAXS (Fig. 3); the experimental spectra were adjusted considering spherical NPs with a normal distribution of radii. The best fit to the experimental GISAXS spectra was obtained for size distributions with an AR of 2.91 nm and RD of 3.37 nm for Au and an AR of 3.25 nm and RD of 3.07 nm for Cu. It can be noted that the resulting average radii are in good agreement with the ones obtained by TEM, while larger RD values are obtained from GISAXS.

Finally, the NPs' radius distributions were estimated from fitting the OES spectra (Fig. 4) using the method described earlier (a software named MieLab was developed to make calculations easier and will be made publicly available at http://scattering.sourceforge.net/). The best fits were obtained for normal distributions of radii with an AR of 2.85 nm and RD of 3.28 nm for Au and an AR of 3.35 nm and RD of 3.31 nm for Cu. Again the obtained average radii are in good agreement with the previous results, and the RD values are larger than the ones obtained from TEM.

In order to present the obtained results in a way that is easier to understand, we plotted in Fig. 5 the normal probability density obtained with the three techniques for Au and Cu. For both metals, the AR are very similar, and the RD values are almost equal for GISAXS and OES and are smaller for TEM. From these results, it is clear that the fitting of the OES spectra (by the method described above) is indeed very accurate, because it yields almost the same values as GISAXS, which is one of the more accurate methods to determine the size distribution of ensembles of particles. This is an important result since, in the case of optically transparent mediums such as glasses containing a dilute set of metallic NPs, the OES has several advantages over SAXS/GISAXS; it is easier to perform, it has fewer restrictions for the samples (they can be considerably thicker, and there are no limitations concerning the in-depth location of the NPs), the required equipment is considerably cheaper, and it can be measured *in situ* (in an easier way). In the case of TEM, satisfactory average radii are obtained, but RD is considerably underestimated, probably because not enough NPs were counted. Besides, the sample preparation for TEM is harder than for the other two methods, and the required equipment is also expensive. From these results, one can conclude that, although TEM is very useful to determine the shape and crystallographic structure of NPs, GISAXS/SAXS and OES provide more precise results of the NPs size distribution function, this being a consequence of the much larger number of particles probed by the latter techniques.

5. Conclusions

We have described a method to estimate the size distribution of metallic NPs from the OES spectra based in Mie's theory and an optimization algorithm. We have shown that, for two different metals embedded

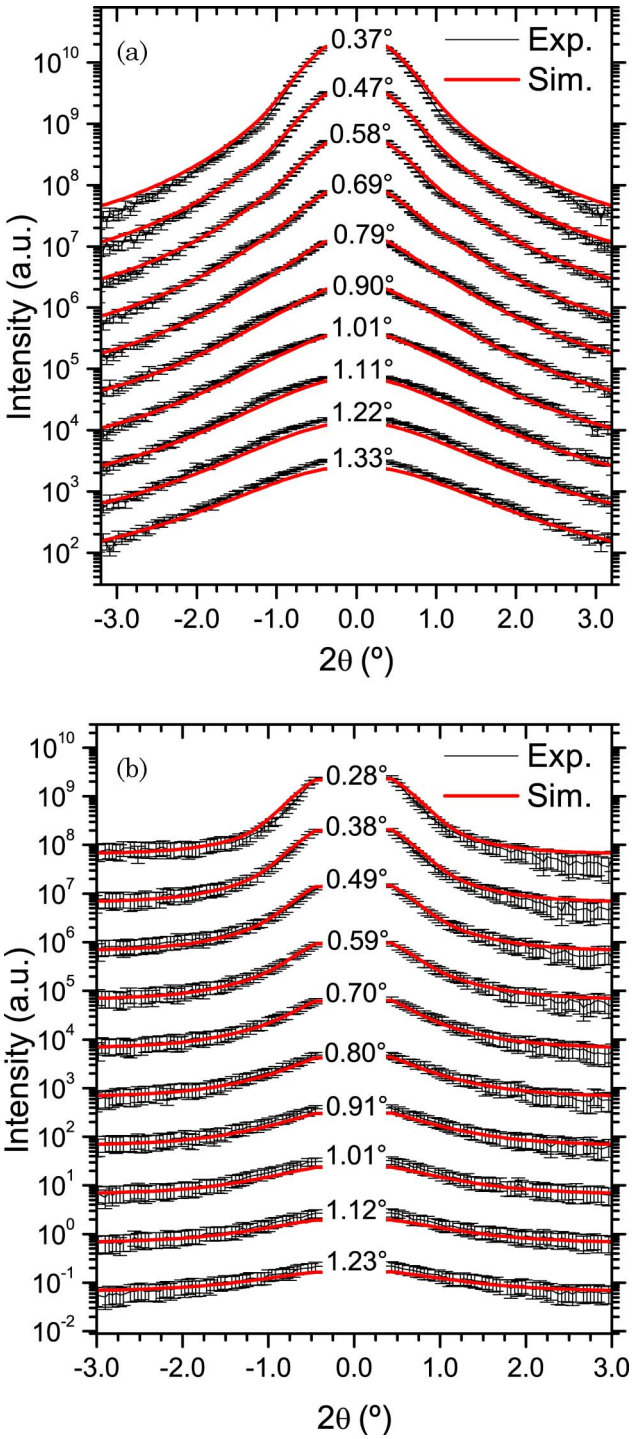

Fig. 3. (Color online) Experimental GISAXS intensity profiles (symbols) and best fit to experimental data (continuous curves) for (a) Au and (b) Cu adjusted considering spherical NPs with a normal distribution of radii. The curves are shifted by increasing powers of 10 for clarity. The α_f value for each profile is indicated in the figure.

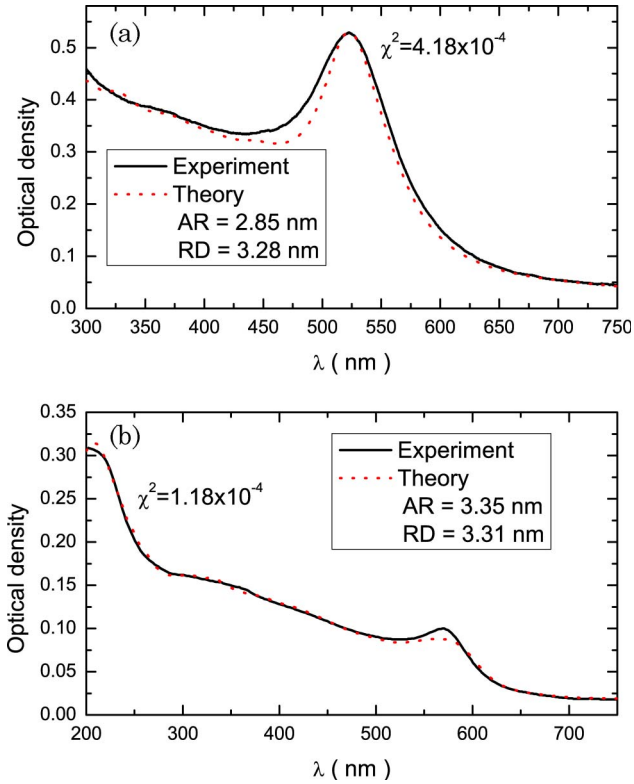

Fig. 4. (Color online) Fitting the OES spectra for (a) Au and (b) Cu, showing that an excellent agreement is obtained between the experimental spectra (continuous black curves) and the simulated ones (dotted red curves) for the given values of AR and RD. A background (assumed to be the OD of unimplanted silica) was added to the simulated spectra.

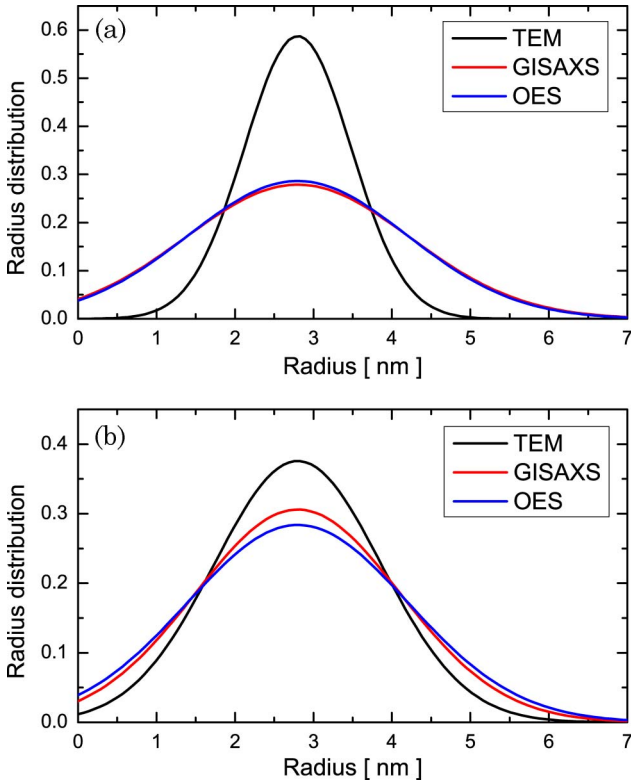

Fig. 5. (Color online) Radius distributions obtained for (a) Au and (b) Cu from TEM (black curve), GISAXS (red curve), and OES (blue curve).

in silica, the obtained results are very similar to the ones obtained by GISAXS and TEM, two of the more widely used methods for this purpose. For the systems studied in this work, very good agreement was obtained by the three techniques when determining the AR, but TEM considerably underestimates the radius distribution; this discrepancy in the RD values obtained by TEM is probably an effect of not sampling enough particles (or different regions) in the samples. Although SAXS/GISAXS and TEM are frequently used for measuring particle size distributions, they both have some disadvantages when compared with OES, due to the sample preparation and expensive facilities required. Therefore optical absorption measurements offer an attractive method to determine the radius distribution of metallic NPs from the analysis of the absorbance measurements, which can be performed with any commercial spectrophotometer, achieving rapid, accurate results with a low cost.

We thank K. López and F. J. Jaimes for the accelerator operation, J. G. Morales for the sample preparation, L. Rendón-Vázquez for TEM assistance, and the Brazilian National Synchrotron Light Laboratory for its support. O. Peña is grateful to Dirección General de Asuntos del Personal Académio, UNAM for extending postdoctoral fellowship. This work was partially supported by Dirección General de Asuntos del Personal Académio-Universidad Nacional Autonóma de México project IN-119706-3.

References

1. F. Tihay, G. M. Pourroy, A. C. Roger, and A. Kienneman, "Effect of Fischer–Tropsch synthesis on the microstructure of Fe–Co-based metal/spinel composite materials," Appl. Catal. A **206**, 29–42 (2001).
2. P. Mazzoldi, G. W. Arnold, G. Battaglin, F. Gonella, and R. Haglund, Jr., "Metal nanocluster formation by ion implantation in silicate glasses: nonlinear optical applications," J. Nonlinear Opt. Phys. Mater. **5**, 285–330 (1996).
3. C. W. White, J. D. Budai, S. P. Withrow, J. G. Zhu, E. Souder, R. A. Zuhr, A. Meldrum, D. J. Hembree, Jr., D. O. Henderson, and S. Prawer, "Encapsulated semiconductor nanocrystals formed in insulators by ion beam synthesis," Nucl. Instrum. Methods Phys. Res. Sect. B **141**, 228–240 (1998).
4. E. Borsella, M. A. Garcia, G. Mattei, C. Maurizio, P. Mazzoldi, E. Cattaruzza, F. Gonella, G. Battaglin, A. Quaranta, and F. D'Acapito, "Synthesis of GaN quantum dots by ion implantation in dielectrics," J. Appl. Phys. **90**, 4467–4473 (2001).
5. L. Pavesi, L. D. Negro, C. Mazzoleni, G. Franzo, and F. Priolo, "Optical gain in silicon nanocrystals," Nature **408**, 440–444 (2000).
6. J. Yguerabide and E. E. Yguerabide, "Resonance light scattering particles as ultrasensitive labels for detection of analytes in a wide range of applications," J. Cell. Biochem. Suppl. **84**, 71–81 (2001).
7. C. Sünnichsen and A. P. Alivisatos, "Gold nanorods as novel nonbleaching plasmon-based orientation sensors for polarized single-particle microscopy," Nano Lett. **5**, 301–304 (2005).

8. A. Oliver, J. C. Cheang-Wong, J. Roiz, L. Rodríguez-Fernández, J. M. Hernández, A. Crespo-Sosa, and E. Muñoz, "Metallic nanoparticle formation in ion-implanted silica after thermal annealing in reducing or oxidizing atmospheres," Nucl. Instrum. Methods Phys. Res. Sect. B **191**, 333–336 (2002).
9. S. Eustis and M. A. El-Sayed, "Determination of the aspect ratio statistical distribution of gold nanorods in solution from a theoretical fit of the observed inhomogeneously broadened longitudinal plasmon resonance absorption spectrum," J. Appl. Phys. **100**, 044324 (2006).
10. L. B. Scaffardi, N. Pellegri, O. de Sanctis, and J. O. Tocho, "Sizing gold nanoparticles by optical extinction spectroscopy," Nanotechnology **16**, 158–163 (2005).
11. U. Kreibig, B. Schmitz, and H. D. Breuer, "Separation of plasmon-polariton modes of small metal particles," Phys. Rev. B **36**, 5027–5030 (1987).
12. M. V Roldán, L. B. Scaffardi, O. de Sanctis, and N. Pellegri, "Optical properties and extinction spectroscopy to characterize the synthesis of amine capped silver nanoparticles," Mater. Chem. Phys. **112**, 984–990 (2008).
13. J. Nocedal, "Updating quasi-Newton matrices with limited storage," Math. Comput. **35**, 773–782 (1980).
14. R. H. Byrd, P. Lu, and J. Nocedal, "A limited memory algorithm for bound constrained optimization," SIAM J. Sci. Statist. Comput. **16**, 1190–1208 (1995).
15. C. Zhu, R. H. Byrd, and J. Nocedal, "L-BFGS-B: Algorithm 778: L-BFGS-B, FORTRAN routines for large scale bound constrained optimization," ACM Trans. Math. Softw. **23**, 550–560 (1997).
16. M. J. Weber, ed., *Handbook of Optical Materials* (CRC , 2003).
17. C. F. Bohren and D. R. Huffman, *Absorption and Scattering of Light by Small Particles* (Wiley, 1983).
18. O. Peña and U. Pal, "Scattering of electromagnetic radiation by a multilayered sphere," submitted to Comput. Phys. Commun.
19. W. Yang, "Improved recursive algorithm for light scattering by a multilayered sphere," Appl. Opt. **42**, 1710–1720 (2003).
20. M. I. Mishchenko, L. D. Travis, and A. A. Lacis, *Scattering, Absorption, and Emission of Light by Small Particles* (Cambridge University, 2002).
21. R. Lazzari, "IsGISAXS: a program for grazing-incidence small-angle x-ray scattering analysis of supported islands," J. Appl. Crystallogr. **35**, 406–421 (2002).
22. P. B. Johnson and R. W. Christy, "Optical constants of the noble metals," Phys. Rev. B **6**, 4370–4379 (1972).
23. O. Peña, U. Pal, L. Rodríguez-Fernández, and A. Crespo-Sosa, "Linear optical response of metallic nanoshells in different dielectric media," J. Opt. Soc. Am. B **25**, 1371–1379 (2008).
24. F. Gonella, "Nanoparticle formation in silicate glasses by ion-beam-based methods," Nucl. Instrum. Methods Phys. Res. Sect. B **166**, 831–839 (2000).